PERFORMANCE SIMULATIONS FOR A SYNTHETIC APERTURE RADIOMETER MEASURING PEAK SURFACE WIND SPEED IN HURRICANES

Ruba Amarin*[1], Boon Lim[2], James Johnson[1], W. Linwood Jones[1] and Christopher Ruf[2]

1. Central Florida Remote Sensing Laboratory
University of Central Florida; Orlando, FL 32816-2450
2. Space Physics Research Laboratory,
AOSS Dept., University of Michigan, Ann Arbor, MI 48109
* ramarin@mail.ucf.edu, (407) 882-2017

ABSTRACT

The Hurricane Imaging Radiometer, HIRAD, is a microwave remote sensor for improved airborne surveillance of ocean surface winds and rain in hurricanes. HIRAD uses a 1-D synthetic aperture thinned array to image the ocean at four frequencies between 4 – 7 GHz. This paper presents a brief description of the HIRAD array antenna and an analysis of some of the methods used in computing reconstructed brightness temperature, T_b, images. Various aperture taper functions for shaping the synthesized array patterns are discussed along with their application to several representative T_b profiles from simulations of cross-track scans in Hurricane Frances. Requirements in matrix conditioning to improve the image reconstruction process will also be discussed. Results will demonstrate the importance of these two image reconstruction considerations to the image smoothing and spatial resolution trade-off and to the Gibbs phenomenon ringing artifacts from the Fourier inversion process.

1. INTRODUCTION

The Hurricane Imaging Radiometer, HIRAD, is a next generation Stepped Frequency Microwave Radiometer, SFMR, [1] for improved airborne surveillance of ocean surface winds and rain in hurricanes. HIRAD is a multi-frequency microwave radiometer at C-band that uses synthetic aperture thinned array radiometry technology to create a 1-D microwave imager that synthesizes brightness temperature images crosstrack and provides real aperture imaging along track. This technology is currently under development at the NASA Marshall Space Flight Center in a collaborative effort with NOAA, the University of Central Florida and the University of Michigan. A horizontal polarization aircraft instrument is planned for completion in 2009. HIRAD has a 0.82 m × 0.57 m, 10 element thinned array, which is comprised of individual multi-frequency, microstrip stacked patch elements that resonate at 4, 5, 6, and 7 GHz. The element spacing in the cross-track direction is optimized at less than λ/2 at 4, 5 and 6 GHz and greater than λ/2 at 7 GHz to maximize spatial resolution but limit grating lobes infringing on the field-of-view. This spacing design produces a field-of-view of ± 61° before the encroachment of grating lobes at 7 GHz [3, 4].

This paper presents analyses and measurement simulations conducted to evaluate the effectiveness of the HIRAD design for observing the peak surface winds in realistic hurricane wind and rain fields. Numerically modeled surface wind and rain fields for Hurricane Frances, 2004 provided by the University of Miami, were used in these analyses [2]. In particular, this paper presents two aspects of brightness temperature, T_b, image reconstruction for the HIRAD array design that relate to estimating peak wind speed in the eyewall region, in heavy rain, and over the full swath. Since crosstrack T_b profiles are produced using antenna patterns that are synthesized in software, array tapering may be used to shape the pattern for smoothing the imaged scene, but at the expense of spatial resolution. Three selected taper functions and their effect on crosstrack imaging will be evaluated here. The second aspect of image reconstruction presented here is a matrix conditioning requirement in the minimum least squares technique used in estimating T_b [4]. This will be discussed in the context of Gibbs phenomenon ringing artifacts due to the Fourier inversion in estimating T_b.

2. APERTURE TAPER AND PATTERN SHAPING

Design studies have been conducted using various image reconstruction algorithms as part of the HIRAD development [4]. The visibility terms that represent the radiometer measurements are computed from,

$$\underset{(N\times 1)}{V} = \underset{(N\times P)}{G} \times \underset{(P\times 1)}{T_b} \qquad (1)$$

where N is the total number of visibilities, P is the number of pixels in the scene, the matrix 'G' characterizes the array, and brightness temperature, T_b, represents the actual brightness temperature scene [4, 5],. The reconstructed T_b scene is given by

$$\hat{T}_b = G' \times V \qquad (2)$$

where $\hat{T}_b$ is the estimated brightness temperature and G' represents the matrix inversion that minimizes the difference between the estimated and actual brightness temperature scenes [4]. For simulation purposes, substituting the expression for the visibility term, the relationship between the actual scene and the measured scene is given by

$$\underset{(P\times 1)}{\hat{T}_b} = \left(\underset{(P\times P)}{G'\times G}\right)\underset{(P\times 1)}{T_b} \qquad (3)$$

and $G'\times G$ represents the synthesized antenna patterns. Each row in $G'\times G$ is a complete pattern at a particular boresight angle.

Various aperture taper functions, or spatial filters, were used to weight the HIRAD G-matrix in simulating visibility measurements and in computing image reconstructions of T_b. Aperture tapers weight the individual visibilities and, effectively, shape the synthesized array patterns, decreasing the sidelobe levels while broadening the main beam. In simulations, selected tapers were applied directly to the G-matrix according to

$$\underset{(N\times 1)}{G_{P\_Taper}} = \underset{(N\times 1)}{G} \times \underset{(N\times 1)}{Taper} \qquad (4)$$

Synthesized patterns at 0 and 60 deg. boresight for the uniform, triangular and Blackman tapers are shown in Fig. 1 for 7 GHz. The uniform taper is just unity weighting for each element (N), the triangular varies linearly from unity at the lowest spatial frequency to zero at the highest, and the Blackman has a somewhat sharper roll-off.

Figure 1 shows that at 0 deg. boresight, the uniform taper has a -6.65 dB first side-lobe level, the triangular taper -13.3 dB, and the Blackman taper -28.92 dB. At 60 deg., the first side lobe levels were -6.3 dB, -11.8 dB, and -26.7 dB, for the uniform, triangular, and Blackman tapers, respectively. The Blackman taper beamwidth is approximately twice that of the uniform taper for both 0 and 60 deg. boresight.

3. IMAGE RECONSTRUCTION SIMULATIONS

The modeled hurricane used in the simulations includes an eye-wall, rain-bands and other realistic structure with a horizontal grid spacing of 0.015 degrees (~1.7 km) in longitude and latitude for the innermost portion of the storm, including the entire eyewall region. The HIRAD simulation constructs cross-track scans at each model grid point, and contiguous scans along the track [6]. Thus, the spatial resolution over the HIRAD field-of-view is the same as the model grid in both cross-track and along track.

Figure 2 shows three typical HIRAD scans simulated from 20 km altitude, which is typical for the NASA ER-2 aircraft. The first scan is taken outside the eyewall region (lower right) where the brightness temperature across the swath is uniform, the second scan (middle) is through the center of the eye and the last scan is in the eyewall region (upper left) where the highest winds occur. The three scans will be referred to as scan 1, 2, and 3, respectively, and the star symbol represents the scan nadir point. The swath width is approximately 70 km at the 20 km altitude.

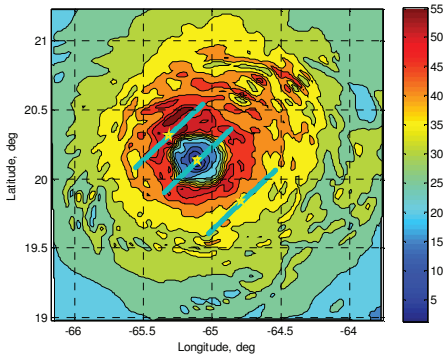

Figure 2 Frances wind field (m/s), HR 24, 31 August, 2004

The uniform, triangular and Blackman tapers were applied to the G-matrix at each frequency for each of the 3 scans, and the HIRAD forward radiative transfer model [7] was used to compute brightness temperature. Figure 3 shows the computed T_b's as a function of earth incidence angle for the three different scans, for each taper.

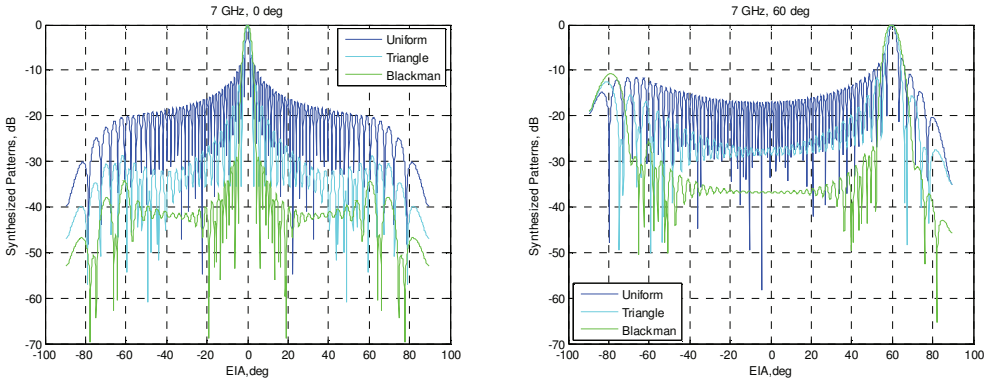

Figure 1 Synthesized antenna patterns for uniform, triangular and Blackman tapers at 7 GHz

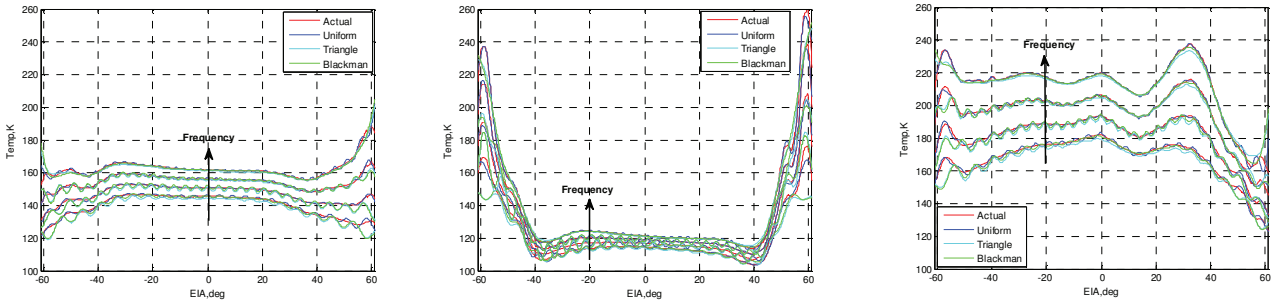

(a) (b) (c)

Figure 3 CFRSL T_{app} using three different tapers at HIRAD frequencies from a 20 km aircraft altitude

The uniform taper is shown to have the best match with the actual brightness temperature over the swath. Results also show the Gibbs phenomenon ringing, with generally increasing amplitude as frequency decreases and maximum amplitude at the swath edges, as expected. The brightness temperature profiles for the triangular and Blackman tapers usually underestimate the actual brightness temperature by as much as ~10 Kelvin in the outer swath.

While computing the reconstructed image, or estimated brightness temperatures, the matrix in the inverse operation in (4) can be "ill-conditioned" causing the inversion to become unstable, and additional information must be introduced into the solution. This process is known as "regularization" and is necessary to obtain a usable inverse. For example, the least square method used in these simulations requires a very simple form of regularization. In (5) an additional small value, the regularization number, γ, was added along the diagonal of the $G \times G^t$ matrix according to,

$$\left(GG^t + \gamma I\right) \tag{5}$$

where I is the identity matrix. The regularization numbers were computed for each frequency so as to minimize the difference between the original scene T_b and the estimated image, $\hat{T}_b$.

Table 1. Regularization numbers for 3 scans using different taper functions

Scan	Freq, GHz	Uniform	Triangular	Blackman
1	4	0	3.6	4
	5	0	4	4.1
	6	0	0.9	0.9
	7	0	3.2	1.6
2	4	1	3.7	4
	5	0	0.4	0.4
	6	0.1	1.1	1.2
	7	0	0	0
3	4	0	3.4	3.6
	5	0.1	3.7	3.6
	6	0.2	0.8	0.9
	7	0	2.8	1

Table 1 summarizes the regularization numbers calculated at each frequency and scan for the different tapers. It is clear that in these examples the regularization numbers required to optimize the image reconstruction are dependent on the scan, which means the magnitude of the T_b's in the scene and the shape of the T_b profile. They are also frequency dependent.

These three dissimilar profiles were selected to get an indication of how sensitive imaging is to regularization, and to get an indication of the potential complexity of producing optimal images in field measurements where the actual T_b scene is unknown, and highly variable in hurricanes. The scenario used in these simulations was to consider these 3 scans to be part of a complete flight pass through the eye of hurricane Frances, which would typically include approximately 200 contiguous scans, and assume a single set of regularization numbers for use with all scans in the pass. This is equivalent to optimizing with respect to one particular T_b scene.

One general observation from the Table is that relatively little regularization is required for any of the scans when the taper is uniform. Nevertheless the T_b profile for Scan 2 at 4 GHz was computed using a Reg. # of zero rather than the optimal Reg. # for this profile of 1.0. Figure 4.a shows the differences between the original T_b at 4 GHz and both of the reconstructed T_b scenes (original – reconstructed), the optimized and the alternative. This simulates a difference between the original (true) scene and the measured scene of ± 2 K or less over most of the swath for optimal regularization, and a difference of ± 2-4 K from 20 deg. out on one side of the swath for the non-optimal case.

Other tests were run with similar results. Scan 2 regularization numbers were used in computing the $\hat{T}_b$ scenes for Scan 3 for both the triangular and Blackman tapers at 5 GHz. The differences between the original T_b and both the reconstructed T_b scenes using the optimal Scan 3 regularization numbers and the alternate Scan 2 numbers are shown in Figs 4.b and c.

These examples show that the magnitude of the ringing artifacts in reconstructed T_b scenes can be exacerbated by

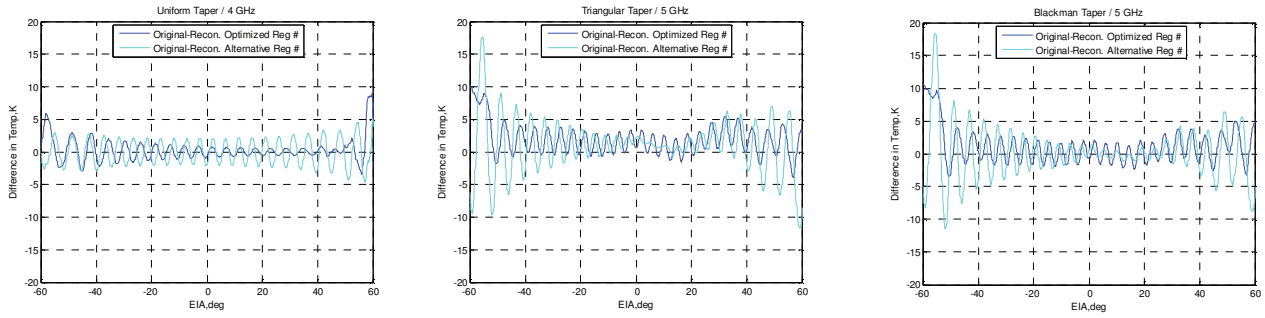

(a) (b) (c)

Figure 4 Differences in T_b a) for Scan 2 using Reg. # = 0, uniform taper at 4 GHz, b) for Scan 3 using a triangular taper at 5 GHz, c) for Scan 3 using a Blackman taper at 5 GHz

non-optimal matrix regularization, and demonstrate the need for optimization for hurricane observations.

Scan 3, which is entirely in the eyewall region, showed the highest retrieved wind speed in the simulations. Figure 5.a shows the difference between the optimal $\hat{T}_b$ and the actual for this scan, and Fig. 5.b shows the retrieved wind speed profiles for this case. This demonstrates the potential for imaging to ± 2 K or better and retrieving wind speed to approximately 2 m/s over most of the swath using the uniform taper (narrowest main beam) but with optimal regularization of the inversion matrix.

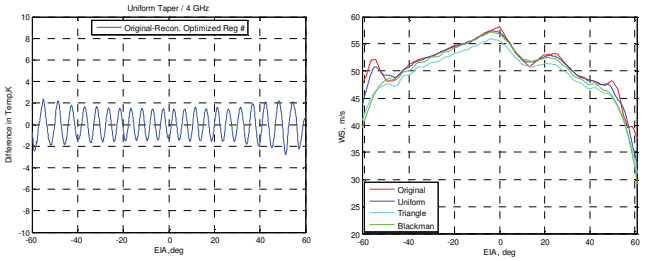

(a) (b)

Figure 5 Scan 3 a) Differences in T_b using optimal regularization, b) Retrieved wind speed

4. CONSLUSIONS

Two aspects of brightness temperature image reconstruction for the HIRAD array have been investigated by simulating a HIRAD pass over hurricane Frances and analyzing estimated T_b scenes for selected crosstrack scans. The effects of array tapering to shape synthesized patterns and lower side lobe levels were evaluated for three selected taper functions, the uniform, the triangular, and the Blackman. Secondly, matrix conditioning requirements in the minimum least squares inversion technique used in estimating T_b were evaluated.

The general conclusions suggested from the results are that the uniform taper should provide the best estimate of wind speed for HIRAD and that some method of optimizing matrix regularization for image reconstruction is needed. Reconstructed brightness temperature scenes are sensitive to the value of the regularization number applied in the inversion process, and the examples presented here show significant effects on estimated T_b. But, these simulations did demonstrate that the uniform taper and optimal inversion in image reconstruction could produce images to ± 2 K and retrievals to ~ 2 m/s.

REFERENCES

[1] E. W. Uhlhorn, P. G. Black, J. L. Franklin, M. Goodberlet, J. Carswell, A. S. Goldstein "Hurricane Surface Wind Measurements from an Operational Stepped Frequency Microwave Radiometer", *American Meteorological Society*, 2007.

[2] Chen, S. S., J. F. Price, W. Zhao, M. A. Donelan, E. J. Walsh, "The CBLAST-Hurricane Program and the Next-Generation Fully Coupled Atmosphere-Wave-Ocean Models for Hurricane Research and Prediction," *Bull. Amer. Meteor. Soc.*, 88(3), 311-317, 2007.

[3] C. Ruf, B. Lim, R. Amarin, J. Johnson, L. Jones, M. C. Bailey, M. James, R. Hood, K. Stephens, V. Rohwedder, "The Hurricane Imaging Radiometer – An Octave Bandwidth Synthetic Thinned Array Radiometer", *Proc. IGARSS 2007*, Barcelona, July 2007.

[4] Boon H Lim, Ruba Amarin, Salem El-Nimri, James Johnson, Linwood Jones and Christopher S Ruf, "Restrictions on the Field of View for an Undersampled 1-D Synthetic Thinned Aperture Radiometry", *Proc. IGARSS 2007*, Barcelona, July 2007.

[5] A. B. Tanner and C. T. Swift, "Calibration of a Synthetic Aperture Radiometer," *IEEE Trans. Geosci. Remote Sensing*, vol. 31, pp. 257-267, Jan. 1993.

[6] S. F. El-Nimri, S. Alsweiss, W. L. Jones, E. Uhlhorn and J. Johnson, "Hurricane Imaging Radiometer Wide Swath Simulation for Wind Speed and Rain Rate", *Presented at. IGARSS 2008*, Boston, 2008.

[7] Ruba A. Amarin, Salem F. El-Nimri, James W. Johnson, W. Linwood Jones, Boon H. Lim and Christopher S. Ruf, "Instrument Design Simulations for Synthetic Aperture Microwave Radiometric Imaging of Wind Speed and Rain Rate in Hurricanes", *Proc. IGARSS 2007*, Barcelona, SP., 2007.